High-mass X-ray Binaries: Illuminating the Passage from Massive Binaries to Merging Compact Objects
Proceedings IAU Symposium No. 346, 2019
L. M. Oskinova, E. Bozzo, T. Bulik & D. Gies, eds.

doi:10.1017/S1743921319002059

Accretion simulations of Eta Carinae and implications to massive binaries

Amit Kashi

Department of Physics, Ariel University, Ariel, POB 3, 40700, Israel
email: kashi@ariel.ac.il

Abstract. Using high resolution 3D hydrodynamical simulations we quantify the amount of mass accreted onto the secondary star of the binary system η Carinae during periastron passage on its highly eccentric orbit. The accreted mass is responsible for the spectroscopic event occurring every orbit close to periastron passage, during which many lines vary and the x-ray emission associated with the destruction wind collision structure declines. The system is mainly known for its giant eruptions that occurred in the nineteenth century. The high mass model of the system, $M_1 = 170 M_\odot$ and $M_2 = 80 M_\odot$, gives $M_{\rm acc} \approx 3 \times 10^{-6} M_\odot$ compatible with the amount required for explaining the reduction in secondary ionization photons during the spectroscopic event, and also matches its observed duration. As accretion occurs now, it surely occurred during the giant eruptions. This implies that mass transfer can have a huge influence on the evolution of massive stars.

Keywords. accretion, accretion disks — stars: mass loss — stars: variables: other — stars: winds, outflows — methods: numerical — (stars:) binaries: general

1. Introduction

Simulating accretion in a binary stellar system entangles many physical processes and requires special treatment. Most accretion simulations are performed in the context of accretion into compact objects that do not have winds at all. There are challenges in this regime of accretion as well, especially if the accretor is a NS with strong magnetic fields. In this case the accretion flows to the magnetosphere and later tunneled along the dipole field onto the magnetic poles, a process that functions as a bottleneck and significantly reduces the accretion rate (compared to conventional disk accretion or wind accretion). If stars are involved they are usually the donors and not the accretors, and even if they accrete they have negligible wind. Massive interacting binary systems, with accretors that have their own winds, are different. Most obviously, since in those systems both stars eject winds, the winds collide.

First 3D simulations of colliding winds were performed for systems such as γ^2 Vel and WR 140 (Folini & Walder 2000, 2002; Walder & Folini 2000, 2002, 2003). These simulations showed the formation of the pinwheel structure of the colliding winds, explained the variability obtained in x-ray, and demonstrated the formation of instability and clumping. The resolution in those early simulations was not high enough to obtain the small-scale structure close to the stars. These simulations and their follow-ups dealt with colliding winds of comparable momentum. However, cases in which one of the stellar winds is much stronger than the other, to the extent that the star with the weaker wind accretes, have not been explored.

An extreme example for a colliding winds system is η Carinae (η Car). The system is composed of a very massive star at late stages of its evolution, the primary, and a hotter and less luminous star, the secondary (Davidson & Humphreys 1997, 2012).

The binary system has a highly eccentric orbit (e.g., Davidson *et al.* 2017), and strong winds (Akashi *et al.* 2006) resulting in unique period of strong interaction every 5.54 years during periastron passage known as the spectroscopic event. During the event many spectral lines and emission in basically all wavelengths show rapid variability (e.g., Davidson & Humphreys 2012; Mehner *et al.* 2015 and many references therein). The x-ray intensity, which also serves as an indicator to the intensity of wind interaction, drops for a duration of a few weeks, changing from one spectroscopic event to the other (Corcoran *et al.* 2015). The last three spectroscopic events showed different spectral features, and reflected a trend in the intensities of various lines (Mehner *et al.* 2015; Davidson *et al.* 2018a). Observations of spectral lines across the 2014.6 were interpreted as weaker accretion onto the secondary close to periastron passage compared to previous events, indicating a decrease in the mass-loss rate from the primary star. This 'change of state' of the primary was already identified by Davidson *et al.* (2005), and theoretically explained by Kashi *et al.* (2016).

Soker (2005b) interpreted the line variations during spectroscopic events as a result of accreting clumps of gas onto the secondary near periastron passages, disabling its wind. The suggestion was later developed to a detailed model accounting for different observations in the accretion model framework (Akashi *et al.* 2006; Kashi & Soker 2009a). An estimate of the amount of accreted mass during the spectroscopic event was first obtained by Kashi & Soker (2009b), who found that accretion should take place close to periastron and the secondary should accrete $\sim$ few $\times$ 10^{-6} $M_{\odot}$ each cycle.

Previous grid-based simulations (Parkin *et al.* 2009, 2011) and SPH simulations (Okazaki *et al.* 2008; Madura *et al.* 2013) of the colliding winds did not obtain accretion onto the secondary. Teodoro *et al.* (2012) and Madura *et al.* (2013) advocated against the need of accretion in explaining the spectroscopic event. The resultion of their simulations was too low to capture the important phsyics of clumping and fragmentation as a result of instabilities and thus they did not obtain accretion.

Higher resolution 3D hydrodynamical numerical simulations (Akashi *et al.* 2013) found that a few days before periastron passage clumps of gas are formed due to instabilities in the colliding winds structure, and some of them flow towards the secondary. The clumps reached the secondary wind injection zone, implying accretion. However, the resolution of their simulation was still not good enough to see the accretion itself.

The final evidence for accretion came from the simulations of Kashi (2017), that showed the destruction of the colliding winds structure into filaments and clumps that later were accreted onto the secondary. Kashi (2017) demonstrated that dense clumps are crucial to the onset of the accretion process. The clumps were formed by the smooth colliding stellar winds that developed instabilities that later grew into clumps (no artificial clumps were seeded). This confirmed the preceding theoretical arguments by Soker (2005a,b) who suggested accretion of clumps. Furthermore, as the simulations in Kashi (2017) included a radiation transfer unit which treats the photon-gas interaction, so the momentum of the accreted gas is being changed appropriately along its trajectory. It thus quantitatively showed that radiative braking cannot prevent the accretion, by that confirming theoretical arguments given by Kashi & Soker (2009b).

2. Simulations results

We tested four approaches to understand the way the secondary wind would respond to the high accretion rate: (1) Approaching gas removal: removing dense gas that reaches the secondary wind injection region, and replacing it by fresh secondary wind with its regular mass loss and velocity. Namely, we do not make any changes to secondary wind and let it continue to blow as if the accreted gas did not cause any disturbance. (2) Exponentially reduced mass loss: reducing the mass loss rate of the secondary as it

https://doi.org/10.1017/S1743921319002059 Published online by Cambridge University Press

approaches periastron passage. This is an artificial approach that does not relate to the actual accretion situation in the simulation, and does not allow recovery of the secondary wind and was used only for comparison. (3) Accretion dependent mass loss: dynamically changing the mass loss rate of the secondary wind in response to the mass that has been accreted. We lowered $\dot{M}_2$ by changing the density of the ejected wind by the *extra* density of the accreted gas, namely

$$\frac{d\dot{M}_{2,\rm eff}}{d\Omega}=\frac{d\dot{M}_2}{d\Omega}\frac{\rho_u(\Omega)-[\rho_a(\Omega)-\rho_u(\Omega)]}{\rho_u(\Omega)}=\frac{d\dot{M}_2}{d\Omega}\left(2-\frac{\rho_a(\Omega)}{\rho_u(\Omega)}\right), \tag{2.1}$$

where Ω is a solid angle, $d\dot{M}_2/d\Omega$ is the differential mass loss of the secondary, $\rho_u(\Omega)$ is the undisturbed density of the secondary wind as if it blows without the interruption of accreted gas, and $\rho_a(\Omega)$ is the density of the incoming accreted gas. This approach gives non-isotropic mass loss rate which depends on the direction from where accreted gas parcels arrived. (4) No intervention: not changing the mass loss rate of the secondary and not removing any accreted gas from the simulation. Cells in the secondary wind injection zone where dense blobs arrive are not replaced by fresh secondary wind.

For each approach we measured the duration of accretion and calculates the accreted mass according to the following scheme. With no accretion, the density in the injection zone of the wind should be $\rho_u(r)=\dot{M}_2/4\pi r^2 v_2$. As the simulations ran, high density clumps and filaments approached the injection zone of the secondary wind and even the cells of the secondary itself. Whenever the actual density $\rho_{a,\rm cell}$ in a cell in the injection zone increased above the expected undisturbed value of $\rho_{u,\rm cell}$, we counted the extra mass as accreted, so that the contribution to the accreted mass is

$$\Delta M_{\rm acc}=(\rho_{a,\rm cell}-\rho_{u,\rm cell})V_{\rm cell}, \tag{2.2}$$

where $V_{\rm cell}$ is the volume of the cell. We then summed all the contributions from all cells in the injection zone to obtain the total mass accreted for that time step.

We found that accretion is obtained for both the conventional mass model ($M_1=120M_\odot, M_2=30M_\odot$) and the high mass model ($M_1=170M_\odot, M_2=80M_\odot$; Kashi & Soker 2016). For the high mass model the stronger secondary gravity attracts the clumps and we get higher accretted mass of $M_{\rm acc}\simeq$ few$\times10^{-6}M_\odot$ yr^{-1} and longer accretion periods, in the order of a month, which much better match the observed ones. We also calculated the increase in optical depth in any line of sight and the reduction in the effective temperature ($T_{\rm eff}$) as a result. Observations of lines during the spectroscopic event indicate ionizing radiation from the secondary equivalent to that of a star with $T_{\rm eff}\lesssim 25\,000$K. We therefore concluded that the approach that best fits observation of the spectroscopic event is approach (4). Namely, our simulations are able to start accretion and shut it down without needing a prescription code to intervene with the natural process. For reasonable and even high mass loss rates, only the high-mass model matched the observed decline in $T_{\rm eff}$ (Fig. 1).

An important parameter we studied is the mass loss rate of the primary, for which we used values within the range explored in the literature (see Kashi 2017). We demonstrated that the mass loss rate of the primary affects the accretion rate of the secondary in non-linear way, and found strong dependency between the accreted mass and the mass loss rate of the primary. The simulations showed that if the mass loss rate of the primary is lowered by a factor of a few the accretion can stop, and by that supported the claim of Mehner *et al.* (2015), who suggested that following the observed 'change of state', it may well happen that the mass loss rate of the primary will continue to decrease and therefore future spectroscopic events will be very weak or might not occur at all. Our findings show that a close binary companion can significantly influence on the evolution of a massive star, especially at later stages where it may undergo giant episodes of mass loss.

https://doi.org/10.1017/S1743921319002059 Published online by Cambridge University Press

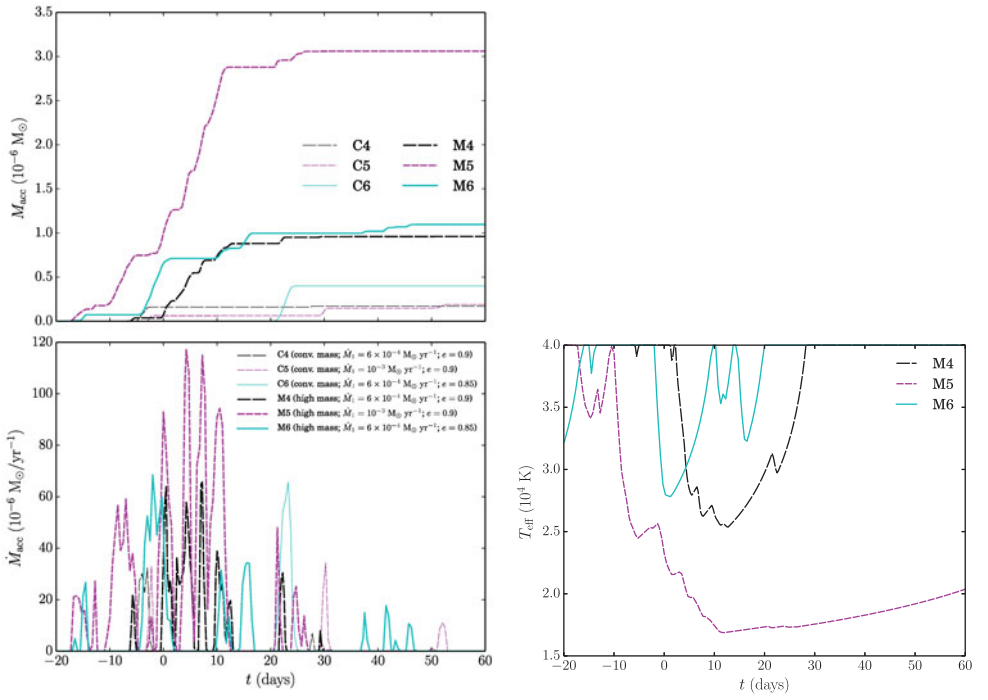

Figure 1. The accreted mass (upper left panel), the accretion rate (lower left panel), and the obtained effective temperature of the secondary, computed for six of our simulations (see parameters in legend). Time is given in days relative to periastron passage ($t = 0$). It can be seen that for the high mass model (M-runs) much more mass is accreted onto the secondary than for the conventional mass model (C-runs). The main reason is the stronger gravity of the secondary. It is also very clear that stronger mass loss rate of the primary (runs C5 and M5) causes a large increase in the accreted mass. The dependence on eccentricity is more complicates as lower eccentricity (runs C6 and M6) means larger periastron distance but also longer periastron passage. These two effects can combine in different ways, making the results difficult to predict. For calculating the effective temperature, first we determine the density $\rho(t)$ by the accreted mass and the mass loss of the secondary, and we then obtain the effective temperature assuming a grey photosphere, averaged over all directions $T^4_{\rm eff}(t) = \frac{4}{3}\left(\tau(t) + \frac{2}{3}\right)^{-1} T^4(\tau = 2/3)$, where we take $T(\tau = 2/3) = 40\,000$ K to be the isotropic effective temperature of the undisturbed secondary,

Another parameter we varied is the eccentricity, for which we also tested $e = 0.85$. This value was favored by Davidson *et al.* (2017) because it gives the smallest possible separation distance at the time when the spectroscopic event begins. It was therefore expected that $e = 0.85$ would produce earlier accretion compared to $e = 0.9$, even though the periastron distance is 50% larger for the smaller eccentricity. Fig. 1 shows our results, confirming that for $e = 0.85$ the accretion duration is indeed longer, and more mass was accreted. Run M6 also showed early accretion exactly as expected by Davidson *et al.* (2017). For the conventional mass model (run C6) we did not see this behavior, because the larger periastron distance and smaller secondary mass combined to reduce the gravitational attraction of the secondary and therefore early accretion could not occur.

3. Conclusions

We conclude that the high mass model for η Car better explains the observations of the decline of lines during the spectroscopic event. Furthermore, we confirm our previous

https://doi.org/10.1017/S1743921319002059 Published online by Cambridge University Press

finding that the radiation of the secondary cannot prevent the accretion of primary gas by radiation braking.

In a future work we intend to explore in more details directional effects of the accreted gas and quantitatively study the angular momentum of the accreted gas and how it effects the binary system at times of spectroscopic events. More effects will be included, especially the acceleration of the winds and the mutual effect of the ratdiations from the stars on the winds.

Acknowledgements

This work used the Extreme Science and Engineering Discovery Environment (XSEDE) TACC/Stampede2 at the service-provider through allocation TG-AST150018. This work was supported by the Cy-Tera Project, which is co-funded by the European Regional Development Fund and the Republic of Cyprus through the Research Promotion Foundation.

References

Akashi, M., Soker, N., & Behar, E. 2006, *ApJ*, 644, 451
Akashi, M. S., Kashi, A., & Soker, N. 2013, *New Astron.*, 18, 23
Corcoran, M. F., Hamaguchi, K., Liburd, J. K., *et al.* 2015, arXiv:1507.07961
Davidson, K., Helmel, G., & Humphreys, R. M. 2018, RNAAS, 2, 133
Davidson, K., & Humphreys, R. M. 1997, *ARA&A*, 35, 1
Davidson, K., & Humphreys, R. M. 2012, *Astrophysics and Space Science Library, Eta Carinae and the Supernova Impostors*, 384
Davidson, K., Ishibashi, K., Martin, J. C., & Humphreys, R. M. 2018, *ApJ*, 858, 109
Davidson, K., Ishibashi, K., Gull, T. R., Humphreys, R. M., & Smith, N. 2000, *ApJL*, 530, L107
Davidson, K., Ishibashi, K., & Martin, J. C. 2017, RNAAS, 1, 6
Davidson, K., Martin, J., Humphreys, R. M., *et al.* 2005, *AJ*, 129, 900
Folini, D., & Walder, R. 2000, *Ap&SS*, 274, 189
Folini, D., & Walder, R. 2002, *Interacting Winds from Massive Stars*, 260, 605
Kashi, A. 2017, *MNRAS*, 464, 775
Kashi, A., Davidson, K., & Humphreys, R. M. 2016, *ApJ*, 817, 66
Kashi, A., & Soker, N. 2009a, *MNRAS*, 397, 1426
Kashi, A., & Soker, N. 2009b, *New Astron.*, 14, 11
Kashi, A., & Soker, N. 2016, *ApJ*, 825, 105
Madura, T. I., Gull, T. R., Okazaki, A. T., *et al.* 2013, *MNRAS*, 436, 3820
Mehner, A., Davidson, K., Humphreys, R. M., *et al.* 2015, *A&A*, 578, A122
Okazaki, A. T., Owocki, S. P., Russell, C. M. P., & Corcoran, M. F. 2008, *MNRAS*, 388, L39
Parkin, E. R., Pittard, J. M., Corcoran, M. F., Hamaguchi, K., & Stevens, I. R. 2009, *MNRAS*, 394, 1758
Parkin, E. R., Pittard, J. M., Corcoran, M. F., & Hamaguchi, K. 2011, *ApJ*, 726, 105
Soker, N. 2005a, *ApJ*, 619, 1064
Soker, N. 2005b, *ApJ*, 635, 540
Teodoro, M., Damineli, A., Arias, J. I., *et al.* 2012, *ApJ*, 746, 73
Walder, R., & Folini, D. 2000, *Ap&SS*, 274, 343
Walder, R., & Folini, D. 2002, *Interacting Winds from Massive Stars*, 260, 595
Walder, R., & Folini, D. 2003, *A Massive Star Odyssey: From Main Sequence to Supernova*, 212, 139